SHORT COMMUNICATIONS

ChemiSTEM Characterization of Bulk Heavy Ion-Irradiated Complex Concentrated Alloys

Calvin Parkin - University of Wisconsin-Madison - cparkin@wisc.edu, caparki@sandia.gov

Conventional nuclear structural alloys show dramatic degradation after hundreds of displacements per atom, which inadequately meet the needs of advanced reactors, triggering exploration of CCAs. Preliminary studies demonstrate the excellent strength, high-temperature performance, and irradiation tolerance of CCA, promoting their candidacy for cladding and duct applications [1-20]. To advance fundamental understanding of the radiation resistance of compositionally complex base matrices, high-temperature irradiations were performed on $Cr_{18}Fe_{27}Mn_{27}Ni_{28}$ and $Cr_{15}Fe_{35}Mn_{15}Ni_{35}$ to high dpa. STEM and super-X were used to characterize the microstructural evolution in terms of defects and chemical segregation.

Experimental or Technical Approach

To investigate the effect of high dose on microstructural evolution, $Cr_{18}Fe_{27}Mn_{27}Ni_{28}$ and $Cr_{15}Fe_{35}Mn_{15}Ni_{35}$ were irradiated at 500°C at the Texas A&M University Accelerator Laboratory using a defocused beam of 5.0 MeV Ni^{2+} ions up to 50, 100, and 200 dpa at the midrange of the plateau region of the damaged profile as computed by the Stopping and Range of Ions in Matter (SRIM) code [21]. Alloy selection, fabrication, preparation, precharacterization, and SRIM inputs are detailed in the references [11] and [3]. Displacement damage and implanted-ion profiles for $Cr_{18}Fe_{27}Mn_{27}Ni_{28}$ are shown in Figure 1. TEM lamellae were extracted using focused ion beam and were examined using a Titan Themis 200 and Thermo Scientific Talos F200X TEMs with EDS systems at the Irradiated Materials Characterization Laboratory and Electron Microscopy Laboratory facilities at Idaho National Laboratory to characterize radiation-induced segregation and void swelling. Voids were measured by hand using ImageJ

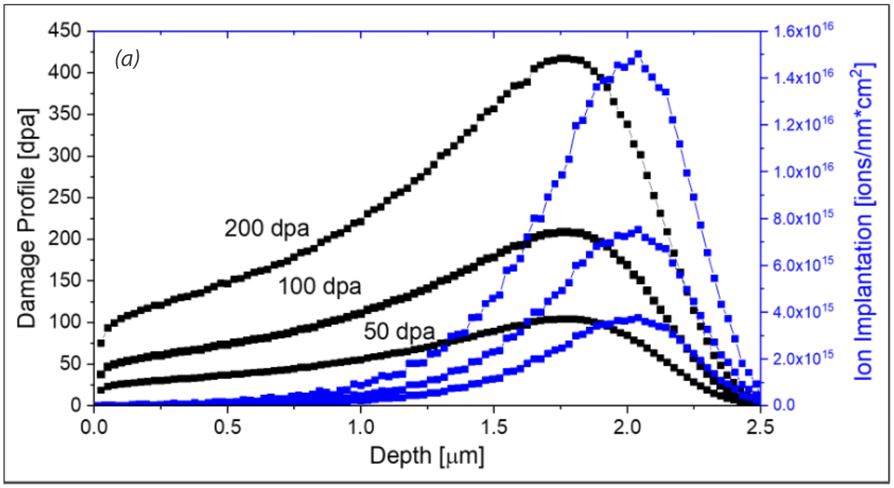

Figure 1. Dpa and ion-implantation profiles for $Cr_{18}Fe_{27}Mn_{27}Ni_{28}$ *generated by SRIM for 5.0 MeV* Ni^{2}*+ ions at 50, 100, and 200 dpa.*

software and using random forest regression image processing software IPSDK by Reactiv'IP [22]. EDS quantifications were performed using the Thermo Scientific Velox software with the default Brown-Powell ionization cross-section model and multipolynomial model for background correction. Lamellae thicknesses were measured by a direct electron method (K2 camera) and a slit width of 15 eV.

Results

All irradiations except $Cr_{15}Fe_{35}Mn_{15}Ni_{35}$ to 50 dpa resulted in void growth, faulted interstitial loops, and chemical redistribution. An example is shown in Figure 2 of a micrograph of $Cr_{15}Fe_{35}Mn_{15}Ni_{35}$ irradiated to 100 dpa, EDS line scans through the irradiated depth and near a void, and chemical maps near a void. The mapping for each depth profile is analyzed and averaged over several microns. EDS profiles are smoothed using an adjacent averaging function. A larger diffuse border of the void in the Mn map indicates vacancies have exchanged more favorably with Mn than with Fe or Cr. The Mn enrichment and Ni depletion just before the displacement peak in the depth profile is consistent across all irradiations except $Cr_{15}Fe_{35}Mn_{15}Ni_{35}$ to 50 dpa and with the irradiations in reference [3]. Swelling levels, as measured manually and by IPSDK, are indicated in Figure 3, which agreed well. $Cr_{15}Fe_{35}Mn_{15}Ni_{35}$ swelled less than $Cr_{18}Fe_{27}Mn_{27}Ni_{28}$ with increasing dosage and experienced less redistribution of Mn with depth. All EDS results indicate Ni becomes enriched near the periphery of voids. A relrod contrast revealed a population of faulted dislocation loops (Figure 4). The average diameter, number density, and dislocation line density are shown in Table 1.

Table 1. Average faulted loop diameter, loop number density, and dislocation density in CCAs irradiated to 50, 100, and 200 dpa at 500°C. [14].

	Loop Diameter [nm]			Number Density $[m^{-3}]$			Dislocation Line Density $[cm^{-2}]$		
dpa	*50*	*100*	*200*	*50*	*100*	*200*	*50*	*100*	*200*
$Cr_{18}Fe_{27}Mn_{27}Ni_{28}$	*11 ± 6*	*3 ± 2*	*6 ± 3*	4.83×10^{21}	1.27×10^{23}	5.57×10^{22}	1.69×10^{10}	1.37×10^{11}	9.84×10^{10}
$Cr_{15}Fe_{35}Mn_{15}Ni_{35}$	*11 ± 5*	*5 ± 2*	*7 ± 3*	2.0×10^{21}	3.74×10^{22}	1.01×10^{22}	2.76×10^{10}	5.6×10^{10}	2.31×10^{10}

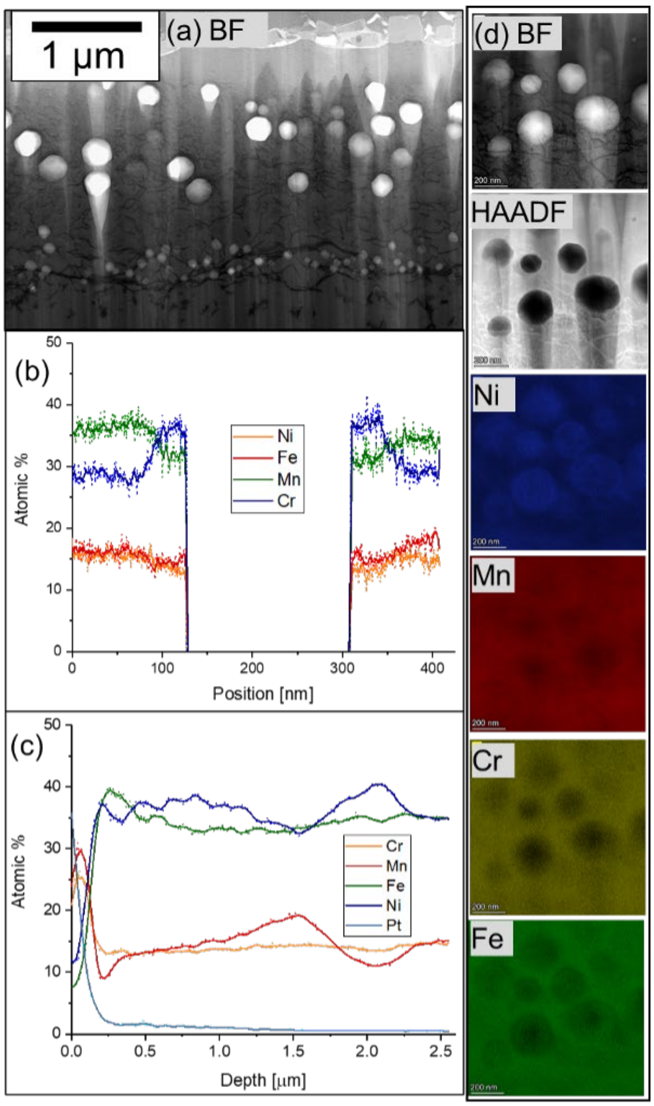

Figure 2. (a) Slightly underfocused micrograph of voids in $Cr_{15}Fe_{35}Mn_{15}Ni_{35}$ irradiated to 100 dpa at 500°C. (b) Super-X EDS linescan across void. (c) Super-X EDS line scan through irradiation depth. (d) Bright-field, HAADF, and super-X EDS maps showing Ni enrichment.

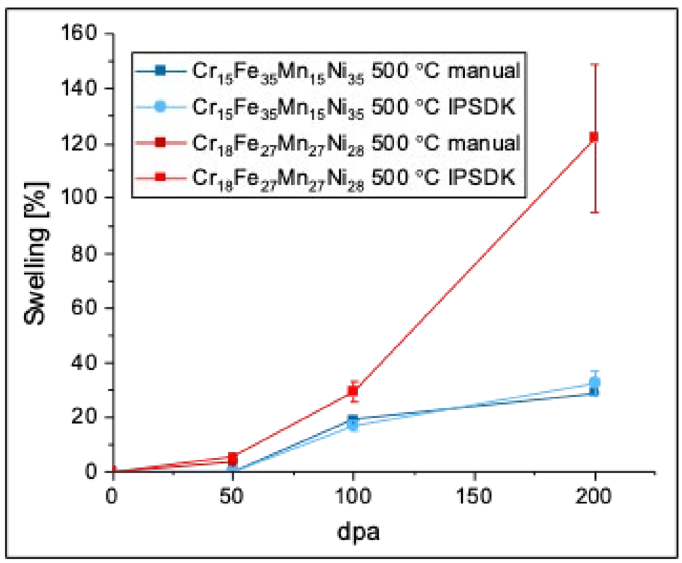

Figure 3. Swelling levels from irradiations comparing manual void measurement to IPSDK software measurement and $Cr_{18}Fe_{27}Mn_{27}Ni_{28}$ to $Cr_{15}Fe_{35}Mn_{15}Ni_{35}$.

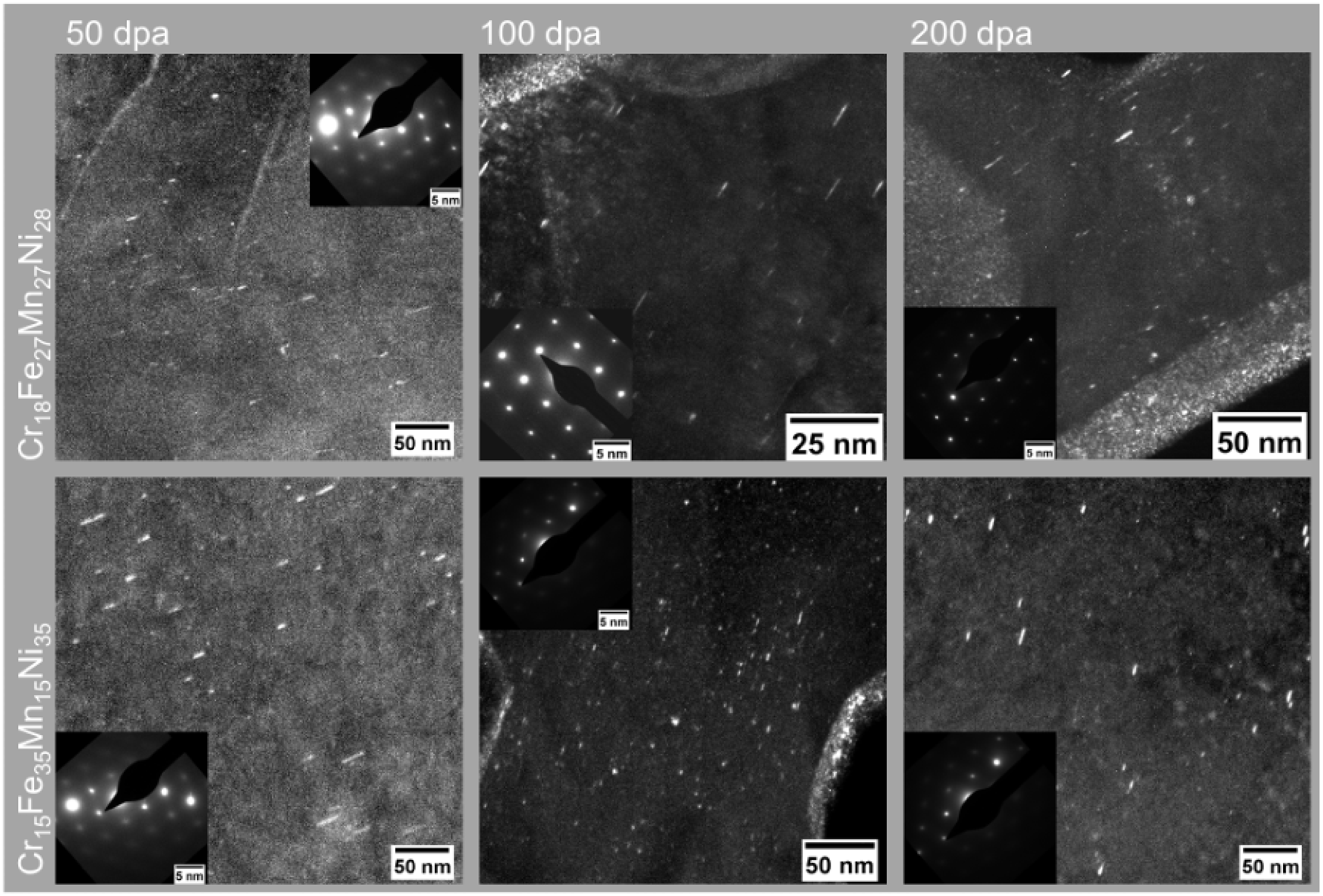

Figure 4. Faulted loops observed in $Cr_{18}Fe_{27}Mn_{27}Ni_{28}$ and $Cr_{15}Fe_{35}Mn_{15}Ni_{35}$ at 50, 100, and 200 dpa.

Discussion/Conclusion

Void nucleation, growth, and chemical redistribution in $Cr_{18}Fe_{27}Mn_{27}Ni_{28}$ and $Cr_{15}Fe_{35}Mn_{15}Ni_{35}$ at various dpa were consistent with the 75 dpa irradiations in reference [3]. Depth-dependent Mn redistribution indicates that vacancies diffuse preferentially via Mn-exchange. Ni exhibits the opposite behavior, effectively diffusing alongside vacancies and enriching the area around voids. Ni enrichment near voids has been observed previously in reference [23], which also has reported Mn depletion near voids and attributed some swelling differences to vacancy mobility. By tailoring the Mn-content, the vacancy mobility can be tuned to prolong void nucleation and promote void-swelling resistance of the base matrix in future alloy design endeavors.

References

[1.] Miracle, D., and O. Senkov. 2017. "A Critical Review of High Entropy Alloys and Related Concepts." Acta Materialia 122: 448–511.

[2.] Kumar, N.A.P.K., et al. 2016. "Microstructural Stability and Mechanical Behavior of FeNiMnCr High Entropy Alloy under Ion Irradiation." Acta Materialia 113: 230–244.

[3.] Parkin, C., et al. 2022. "Phase Stability, Mechanical Properties, and Ion Irradiation Effects in Face-Centered Cubic FeCrMnNi Compositionally Complex Solid-Solution Alloys at High Temperatures." Journal of Nuclear Materials 565: 153733.

[4.] Egami, T. et al. 2013. "Irradiation Resistance of Multicomponent Alloys." Metallurgical and Materials Transactions A 45: 180–183.

[5.] Jin, K., et al. 2016. "Effects of Compositional Complexity on the Ion-Irradiation Induced Swelling and Hardening in Ni-Containing Equiatomic Alloys." Scripta Materialia 119: 65–70.

[6.] Yang, T., et al. 2018. "Irradiation Responses and Defect Behavior of Single-Phase Concentrated Solid Solution Alloys." Journal of Materials Research 33 (19): 3077–3091.

[7.] Lu, C., et al. 2016. "Enhancing Radiation Tolerance by Controlling Defect Mobility and Migration Pathways in Multicomponent Single-Phase Alloys." Nature Communications 7: 13564.

[8.] Lu, C., et al. 2017. "Radiation-Induced Segregation on Defect Clusters in Single-Phase Concentrated Solid-Solution Alloys." Acta Materialia 127: 98–107.

[9.] Jin, K. and H. Bei. 2018. "Single-Phase Concentrated Solid-Solution Alloys: Bridging Intrinsic Transport Properties and Irradiation Resistance." Frontiers in Materials 5 (26).

[10.] Shi, S., et al. 2018. Evolution of Ion Damage at 773K in Ni- Containing Concentrated Solid-Solution Alloys." Journal of Nuclear Materials 501: 132–142.

[11.] Parkin, C., et al. 2020. "In-Situ Microstructural Evolution in Face-Centered and Body-Centered Cubic Complex Concentrated Solid-Solution Alloys under Heavy Ion Irradiation." Acta Materialia 198: 85–99.

[12.] Chen, W.-Y., et al. 2018. "Irradiation Effects in High Entropy Alloys and 316H Stainless Steel at 300°C." Journal of Nuclear Materials 510: 421–430.

[13.] Li, C., et al. 2019. "Neutron Irradiation Response of a Co-Free High Entropy Alloy." Journal of Nuclear Materials 5127: 151838.

[14.] Egami, T. 2015. "Local Electronic Effects and Irradiation Resistance in High-Entropy Alloys." The Journal of The Minerals, Metals & Materials Society 67 (10): 2345–2349.

[15.] Körmann, F., et al. 2017. "Phonon Broadening in High Entropy Alloys." npj Computational Materials Science 3: 36.

[16.] Zhang, Y., et al. 2016. "Influence of Chemical Disorder on Energy Dissipation and Defect Evolution in Advanced Alloys." Journal of Materials Research 31 (16): 2363–2375.

[17.] Zhao, S. et al. 2019. "Frenkel Defect Recombination in Ni and Ni-Containing Concentrated Solid-Solution Alloys." Acta Materialia 173: 184–194.

[18.] Caro, M., et al. 2015. "Lattice Thermal Conductivity of Multi-Component Alloys." Journal of Alloys and Compounds 648: 408–413.

[19.] Béland, L., Y. Osetsky, and R. Stoller. 2016. "The Effect of Alloying Nickel with Iron on the Supersonic Ballistic Stage of High Energy Displacement Cascades." Acta Materialia 116: 136–142.

[20.] Zhang, Y., et al. 2015. "Influence of Chemical Disorder on Energy Dissipation and Defect Evolution in Concentrated Solid Solution Alloys." Nature Communications 6: 8736.

[21.] Stoller, R., et al. 2019. "Erratum to 'On the use of SRIM for computing radiation damage exposure [Nucl. Instrum. Methods Phys. Res. B 310 (2013) 75–80].'" Nuclear Instruments and Methods in Physics Research B 459: 196–197.

[22.] Reactiv'IP Smart Image Processing. 2022. "Image Processing." Accessed February 2023. https://www.reactivip.com/image-processing/.

[23.] Wang, X., et al. 2022. "Understanding Effects of Chemical Complexity on Helium Bubble Formation in Ni-Based Concentrated Solid Solution Alloys Based on Elemental Segregation Measurements." Journal of Nuclear Materials 569: 153902.

Publications:

[1.] Parkin, C., et al. (submission pending). "Dose and Temperature Effect in CrFeMnNi Compositionally Complex Solid-Solution Alloys under Heavy Ion Irradiation." Journal of Nuclear Materials.

Distributed Partnership at a Glance

NSUF Institution	Facilities and Capabilities
Idaho National Laboratory	Electron Microscopy Laboratory Irradiated Materials Characterization Laboratory
Texas A&M University	Accelerator Laboratory
Collaborators	
Idaho National Laboratory	Lingfeng He (Co-Principal Investigator)
University of Wisconsin-Madison	Adrien Couet (Co-Principal Investigator)
Degrees Granted	
University of Wisconsin-Madison	Calvin Parkin, Ph.D.